

A materials-based approach for interrogating human prostate cancer cell adhesion and migratory potential using a fluoroalkylsilica (FS) culture surface.

Matthew Nicklin^{1,2}, Graham J. Hickman¹, A. Graham Pockley² & Carole C. Perry^{1}*

¹Biomolecular & Materials Interface Research Group, and the ²John van Geest Cancer Research Centre, School of Science and Technology, Nottingham Trent University, Clifton campus, Clifton Lane, Nottingham, NG11 8NS, UK

Keywords: Epithelial, Mesenchymal, Adhesion, Silica, Surface chemistry.

Abstract

OPCT-1 is a heterogeneous prostate cancer cell line derived from primary (rather than metastatic) disease which contains epithelial, mesenchymal and CD44^{high}/CD24^{low} cancer stem cell (CSC) sub-populations and from which we have previously generated and characterized stable mesenchymal (P4B6B) and epithelial (P5B3) cell sub-populations. In this contribution, we explore the effect of tissue culture surface chemistry (standard tissue culture plastic (TCP) and a fluoroalkylsilica (FS) culture surface with inherently low surface energy) on the phenotype and adherent capacity of mesenchymal and epithelial cell populations. We demonstrate that OPCT-1 cells adherent to FS surfaces comprise both epithelial- and mesenchymal-like populations; a mesenchymal sub-population derived from OPCT1 (P4B6B) poorly adheres to FS and formed

spheroids whereas an epithelial sub-population derived from OPCT1 (P5B3) forms an adherent monolayer. In contrast, P4B6B cells do adhere to FS when co-cultured with P5B3 cells. Taken together, these findings demonstrate that EMT/cell differentiation status dictates cell adhesive capacity and provide a novel insight into the relationship between epithelial and mesenchymal cell populations in metastasis. Importantly, the differences in adherence capacity between P4B6B and P5B3 are not apparent using standard TCP-based culture, thereby highlighting the value of using alternative culture surfaces for studying cell surface interaction/adhesion phenomena and interrogating mechanisms involved in adhesion and detachment of metastatic tumor cells.

Introduction

Approximately 90% of cancer-related deaths are due to aggressive, therapy-resistant disease which has spread from the primary tumor to other tissues. The successful treatment of aggressive cancer is significantly hindered by the high degree of heterogeneity of tumors, which is progressively acquired by genetic alterations and exposure to the local microenvironment [1]. Progress in the management and treatment of aggressive, therapy-resistant metastatic cancers urgently requires a better understanding of the events that enable cells in the primary tumor to acquire migratory potential and be resistant to a form of programmed cell death that occurs in anchorage-dependent (epithelial) cells when they detach from the surrounding extracellular matrix (ECM) - Anoikis.

Epithelial to mesenchymal transition (EMT) represents a molecular and cellular program, during which polarized epithelial cells, which typically interact with the basement membrane in tissue via their basal surface, transition through a range of biochemical and phenotypic changes which result in a mesenchymal phenotype endowed with a heightened ability for migration and invasion, an increased resistance to apoptosis and an increased production of ECM components [2, 3].

Mesenchymal cells typically hold little capacity for cell-cell interaction and are inherently resistant to anoikis [4]. Significant evidence links EMT to therapeutic resistance and tumor recurrence and its role as a potential therapeutic target has therefore gained significant attention [5, 6].

Cells undergoing EMT display profound changes in their cytoskeletal architecture, adopting a non-polarized spindle morphology, which contributes to their ability to migrate and break through the basal membrane. Specifically, they undergo a ‘cadherin switch’, which involves a reduction in E-cadherin expression and an induction of N-cadherin expression [7]. Other classic hallmarks of EMT include reduced expression of the cell-cell adhesion protein β -catenin, and increased expression of the intermediate filament vimentin and mesenchymal transcription factors ZEB-1, SLUG and SNAIL [8, 9]. Tumor cells have also been characterized by ‘stemness’, based on variations in the expression of surface proteins (markers) such as CD44 and CD24, among others [10]. The presence of therapy-resistant stem-like cells having the ability to self-renew and initiate tumors has also been linked to disease progression.

EMT significantly changes the interaction of cells with the ECM, such as the basement membrane [11]. Integrins are important to cell locomotion and adhesion, in that they are the primary receptor system used by cells to bind and respond to the ECM [12]. Integrin expression is therefore a key determinant of overall cellular adherence capability [12, 14]. During EMT, the expression profiles of many integrin receptors change [15]. As epithelial cells acquire mesenchymal characteristics, expression of epithelial integrins (such as A β 1) is downregulated and that of mesenchymal integrins (such as A ν β 3) is induced [11]. During EMT, perturbations of the ECM driven by metalloproteases or alterations in the composition of the ECM composition can also influence cell-ECM interactions mediated *via* integrin receptors [15]. EMT can therefore

alter cell adhesive capacity by adapting the integrin expression profile, as well as by remodeling of the ECM itself.

Adsorption of ECM proteins such as fibronectin (FN), laminin and collagen IV is influenced by surface chemistry, and it is the availability of such ECM proteins at the interface which plays an important role in the manipulation of cell behavior, including cell adhesion and spreading [16]. Tailoring the properties of surfaces such as their chemistry can change the profile of adsorbed proteins at the interface and influence a cell's response to that interface [16, 17]. Thus, cells at different stages of differentiation are likely to present differential biological responses towards specific, chemically defined interfaces. Surface chemistry is therefore a rational means to study the differential adhesive properties of specific tumor sub-populations, alongside the impact they have upon the bulk population [18]. Although tissue culture polystyrene (TCP) is engineered to be highly accommodating for cellular adhesion, studying events involving a loss of cellular adhesion requires surfaces that are less accommodating for cellular adherence.

The ability to control aggregation-disaggregation events *in vitro* using surface defined microenvironments allows the interrogation of different stages within hematogenous metastasis, during which cells break away from the surrounding tissue and population specific responses to be observed. As with drug susceptibility, it is likely that the adherence and tolerance of mesenchymal sub-populations to anoikis will differ when cultured on a given substrate compared to epithelial populations, although this has not yet been directly measured [7, 19]. Previously, we used a low surface energy fluoroalkylsilica (FS) culture surface to study cancer cell aggregation-disaggregation events in serum-supplemented culture, a process attributed (in part) to the inability of FS to adsorb fibronectin (FN) under these conditions [20].

Despite recent advances in detection and treatment, patients continue to die from aggressive, therapy-resistant metastatic prostate cancer [21, 22]. Herein, we examine how the adherent capacity of epithelial and mesenchymal tumor cell sub-populations differ and influence each other by culturing on FS the heterogeneous prostate cancer cell line OPCT-1 and its clonal epithelial (P5B3) and mesenchymal (P4B6B) progeny that we have previously reported upon and characterized [23]. Our previous studies have shown that OPCT-1 and its clonal progeny are a model of tumor heterogeneity which enables the characteristics of specific sub-populations of interest to be studied in isolation or in co-culture. Combining these differing cell and surface characteristics provides insights into the biology of EMT and cancer metastasis.

Materials and methods

Cell culture and FS surface preparation

The prostatic adenocarcinoma, OPCT-1, was a generous gift from Asterand Bioscience (Royston, UK). This cell line was derived from the primary tumour in a 68-year-old patient with prostate cancer presenting with a TNM stage of T1cN0M0 and a Gleason score of 6 (3+3) [24]. P5B3 and P4B6B cell lines were derived from clonal progeny isolated from OPCT-1, as previously reported [23]. Cell lines were used within 10 passages of the master stock. Keratinocyte serum free medium (KSFM, Fisher cat #17005-042) was supplemented with 10% v/v fetal calf serum (FCS). Medium was not changed during experiments to prevent disruption to the cell-interface dissociation observed upon the FS. Cells were cultured under standard conditions (SC), at 37°C in 5% v/v CO₂ unless otherwise stated. Adherent tissue culture plastics (TCP) were obtained from Sarstedt (Leicester, UK). FS surface preparation followed the protocol as previously reported [20].

Influence of culture surface on proliferation – the MTT assay

OPCT-1, P5B3 and P4B6 cells (0.5×10^5) were seeded to separate TCP/FS surfaces in a 3 mL volume (24-well plate format). To determine background signal, cell free medium was added to both TCP and FS surfaces. At each time point (24-96 h), 300 μ L of the tetrazolium dye MTT 3-(4,5-dimethylthiazol-2-yl)-2,5-diphenyltetrazolium bromide (Sigma cat #M5655, 5 mg/mL in PBS) was added, after which cell culture continued for 2 h. A 2.5 mL aliquot was removed from each well and 500 μ L of 10% w/v SDS in 0.01 M HCl added (to solubilize the formazan product). Plates were incubated under SC overnight. Aliquots of 200 μ L were transferred in triplicate to a clear flat bottom 96-well plate prior to an absorbance measurement at 570 nm, with background subtraction at 690 nm using a TECAN ULTRA spectrophotometer. Corrected absorbance was calculated by subtracting the average signal of background wells from sample wells.

Influence of culture surface on migratory properties - live imaging

OPCT-1, P5B3 and P4B6B cells (1×10^6) were seeded separately onto TCP and FS (6-well format) in 7 mL of medium. Cultures were maintained under SC and plates were imaged using a Leica TCS SP5 inverted laser scanning confocal microscope (LSCM). Bright-field micrographs were taken every 30 min for 96 h, videos were compiled from each point of interest using LAS-AF (Leica). For co-culture experiments interrogating the cross-regulation of responses, this process was performed for 72 h of using P5B3 cells (1×10^6), P4B6B cells (1×10^6) and a 1:1 mixture (1×10^6 total) of these lines. Videos made from live cell imaging data can be viewed in the S.I. S10-17.

EMT status of cell populations - Western blotting

OPCT-1, P4B6B and P5B3 cells (5×10^6) were lysed in 500 μ L of ice cold RIPA buffer (150 mM NaCl, 1% v/v NP-40 Triton, 0.5% w/v Sodium deoxycholate, 0.1% w/v SDS, 50 mM Tris, pH 8.0) supplemented with protease inhibitor cocktail (Sigma cat #8340). Lysates were immediately

sonicated on ice for three 5 min intervals. Further mixing was conducted by repeated pipette aspiration. Cellular debris was removed by centrifugation (10,000 g, 10 min, 4°C), after which protein was quantified using the Bio-Rad DC protein assay (cat #500-0112). For each sample, 30 µg of protein was separated by gel electrophoresis. In each case, blots were run in duplicate to allow for probing of the loading control protein, β-actin. For FN, transfer was conducted overnight at 4°C (30 v), and for other proteins and β-actin for 1 h at RT (100 V). Membranes (nitrocellulose) were washed in TBS and blocked for 1 h in 5% w/v milk powder at RT. Primary antibody was applied in TBS with 5% w/v milk powder and blots were incubated overnight at 4°C with rocking. Membranes were stained for FN using a monoclonal murine anti-fibronectin antibody (clone 10/Fibronectin, BD Biosciences cat #610077, at the recommended dilution) and for EMT proteins using the Cell Signaling Technology EMT Antibody Sampler kit (cat #9782). Membranes were then washed x3 for 5 min in TBS containing 1% v/v Tween 20, followed by application of the secondary Ab in 5% w/v milk powder for 2 h at RT. Detection of FN and β-actin was undertaken using a horseradish peroxidase (HRP)-conjugated polyclonal rabbit anti-mouse Ab (Cell Signaling Technology cat #70765, 1:2000 dilution) and EMT markers using an HRP-conjugated polyclonal goat anti-rabbit IgG from the Cell Signaling Technology EMT Antibody Sampler kit (cat #9782). After washing, secondary antibody binding was detected using the Clarity™ Western ECL substrate (Bio-Rad cat #1705061) and bands identified in reference to a molecular weight ladder (Precision Plus Protein™ WesternC™, Bio-Rad cat #1610376).

EMT status of cell populations - RT-PCR

Lysis of OPCT-1, P4B6B and P5B3 cells and the preparation of RNA were conducted using the RNeasy™ Mini kit and recommended protocol (Qiagen cat #74104). RNA was quantified using a NanoDrop™ spectrophotometer and 2 µg of RNA was used as a template for reverse transcription

(90 min at 38°C, followed by heat inactivation for 5 min at 95°C). cDNA was diluted 1 in 2 with double distilled (dd)H₂O. RT-PCR experiments were undertaken according to the manufacturers protocol using SYBR™ Green (Bio-Rad cat#172-5124) - 40 cycles per experiment on a Qiagen Rotor gene Q instrument. Each 13 µL reaction consisted of 1 µL of cDNA template (40 ng/reaction) or H₂O for no template controls, 0.2 µM of forward and reverse primer and 6.75 µL SYBR™ Green Master mix. Data were analyzed using the PFAFFL method [25]. Relative expression changes in P4B6B and P5B3 were derived from comparing their Ct values to that of OPCT-1, with normalization to the reference gene HPRT. Details regarding primers, cycling conditions etc. can be found in the S.I. S1, 2.

EMT status of cell populations – immunofluorescence staining

OPCT-1, P5B3 and P4B6B cells (1×10^4) were seeded onto fluorescence compatible 96-well plates (BD Biosciences cat #353219) in 200 µL of medium. Plates were incubated for 24 h under SC, after which wells were washed x3 with 300 µL of PBS. Cells were fixed for 15 min with 200 µL of 4% w/v formaldehyde (Sigma cat #F8775) in PBS. Cells were washed x3 with 250 µL of PBS supplemented with 0.1% v/v Tween 20 and then blocked in wash buffer supplemented 10% v/v FCS for 1 h at RT. Primary staining was conducted with 200 µL/well in blocking buffer, overnight at 4°C. Cells were stained for the expression of fibronectin (FN) using a polyclonal rabbit anti-human fibronectin primary antibody (Sigma cat #F3648, 1:400 dilution) and for E-cadherin, vimentin and β-catenin using monoclonal rabbit antibodies (Abs) from the Cell Signalling technology EMT Ab sampler kit (cat #9782), all at the recommended dilution.

Wells were washed x3 with wash buffer and detection binding of primary antibody detected using an FITC-conjugated polyclonal swine anti-rabbit immunoglobulin secondary antibody (Dako cat #F005401-2, now Agilent, 1:40 dilution (in blocking buffer) for 2 h at RT). Plates were

washed once prior to the addition of DAPI (VECTASHIELD™, VECTOR Laboratories cat #H-1200) and imaged using a Leica TCS SP5 LSCM. Z-stacks were prepared for each sample (2 μM steps) with the same laser power/gain between samples. Background signal was assessed by excluding the primary antibody from the staining protocol for each condition (S.I. S3).

Phenotype of cell populations – flow cytometry

The presence of CD44⁺CD24^{-/low} cells was determined by washing OPCT-1, P5B3 and P4B6B cells twice with PBS, after which they were disassociated using Accutase® (Sigma cat #A6964). Cells (1x10⁶) were washed x2 with 1 mL of PBS, pelleted and suspended in 100 μL of PBS. The presence of viable cells was detected by incubating cells for 15 min with 1 mL of Invitrogen LIVE/DEAD® Fixable Violet Dead Cell Stain (ThermoFisher Scientific cat#L34955), after which cells were washed x2 with 1 mL of PBS, suspended in 100 μL of PBS and incubated for 1 h at RT with 5 μL of an FITC-conjugated rat anti-human CD44 monoclonal antibody (mAb) (clone IM7, ThermoFisher cat# eBioscience, 11-0441-82) and an APC-conjugated mouse anti-human CD24 mAb (clone eBioSN3 (SN3 A5-2H10), ThermoFisher cat# 17-0247-41). Cells were washed with 2 mL of PBS and suspended in 500 μL of Beckman Coulter ISOTON™ II diluent prior to analysis using a Beckman Coulter Gallios™ flow cytometer. Individual cells were identified using forward and side light scatter (FSc, SSc) and gated upon based on unstained samples, LIVE/DEAD™ only, LIVE/DEAD™ + CD44, LIVE/DEAD™ + CD24 and LIVE/DEAD™ + CD44 + CD24 (S.I. S4-6). Data were acquired, analyzed and presented using Beckman Coulter Kaluza™ acquisition and analysis software.

For determining vimentin expression, OPCT-1, P5B3 and P4B6B cultures were washed twice with PBS and disassociated using Accutase®. Cells (1x10⁶) were incubated with LIVE/DEAD® Fixable Violet Dead Cell Stain as described above. Cells were washed twice with 1 mL of PBS

and fixed by re-suspending in 2% v/v formaldehyde solution (Sigma cat# F8775) for 15 min at RT. Cells were washed in 2 mL of PBS and permeabilised by suspending in 100 μ L of 0.5% v/v TweenTM 20 in PBS (Sigma cat# P9416). Cells were washed in 2 mL of 0.1% v/v TweenTM 20, in 100 μ L of which they were then resuspended. Cells were then incubated with 10 μ L PE-conjugated murine anti-human vimentin mAb (clone RV202, BD Biosciences cat# 562337) for 1 h at RT. Cells were washed in 2 mL of PBS and suspended in 500 μ L ISOTONTM II diluent prior to analysis, as described. Gating was based on unstained samples, LIVE/DEADTM only and LIVE/DEADTM + vimentin (S.I. S7-9).

For the mesenchymal enrichment studies, 3×10^6 OPCT-1 cells were cultured upon TCP or FS for 48 h in 5 mL of medium (6-well format), following which medium from the FS-based cultures was collected and wells washed x3 with 5 mL of PBS. The wash was added to the collected medium to provide the 'non-adherent' cell fraction. Cells were washed twice in 10 mL of PBS and re-suspended in 2 mL of Accutase[®]. Cells remaining adherent on the FS and TCP surfaces were washed twice with 5 mL of PBS and dissociated using 2 mL of Accutase[®]. Vimentin staining and characterization was then conducted as above. P5B3 and P4B6B co-cultures were disassociated using Accutase[®] and 1×10^6 P5B3, P4B6B and P5B3/P4B6B (mixed 1:1) cells were cultured in triplicate on TCP or FS surfaces for 72 h in a total of 7 mL of medium (6-well format). P4B6B cells cultured on FS were harvested by gentle tapping and processed as described above. These cells were washed x2 and re-suspended in 2 mL of Accutase[®]. Adherent P4B6B, P5B3 and P5B3/P4B6B cells remaining on the culture plates were harvested using Accutase[®] dissociation following three wash cycles with 5 mL of PBS to remove non-adherent cells. Vimentin expression by each cell population was determined as described above.

Statistical analysis.

All figures were prepared using GraphPad Prism 6 unless otherwise stated and data are expressed as mean \pm standard deviation, as appropriate. Statistical differences between relevant experimental groups were examined using the unpaired t-test (*P \leq 0.05, ** P \leq 0.01, ***P \leq 0.001).

Results

Characterization of EMT and CSC markers by OPCT-1, P5B3 and P4B6B cells.

Within the OPCT-1 cell line, a mixture of different cell types can be observed [23]. This includes the typical ‘cobblestone’ morphology of epithelial lines, but also elongated, mesenchymal like cells. IF staining (Fig. 1A) revealed that the OPCT-1 population contained E-cadherin negative and vimentin positive sub-populations, thereby indicating the presence of both epithelial and mesenchymal populations. Variations in the degree of expression of β -catenin and fibronectin (FN) were also observed between cells within OPCT-1, reinforcing this observation [9].

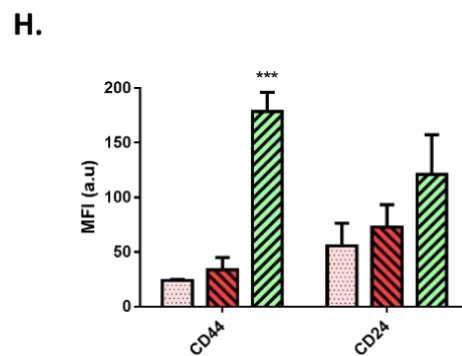
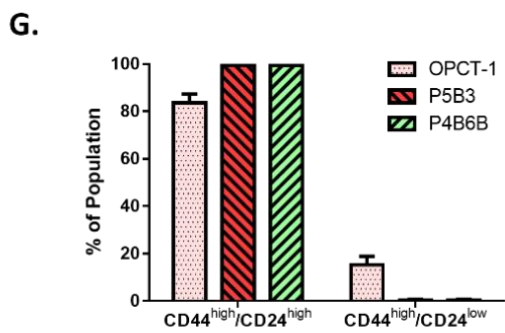
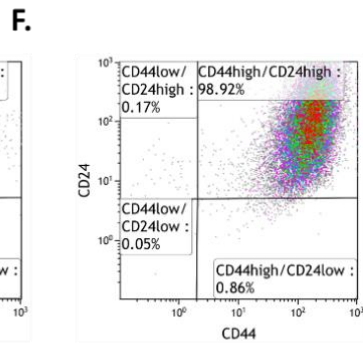
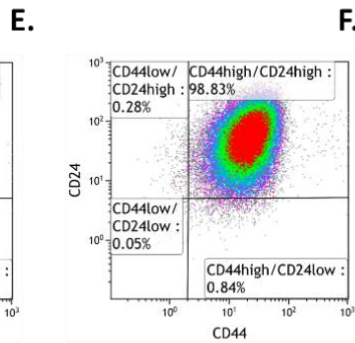
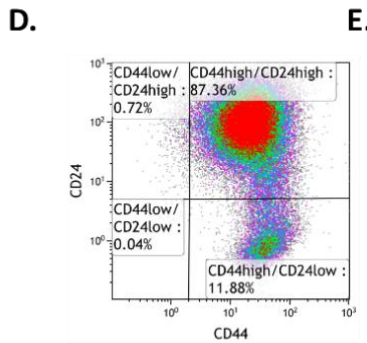
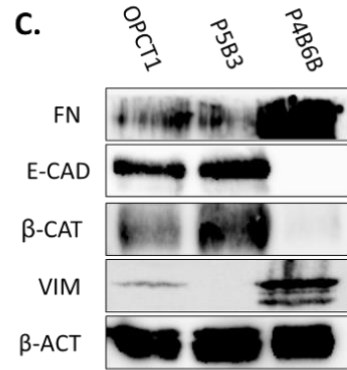
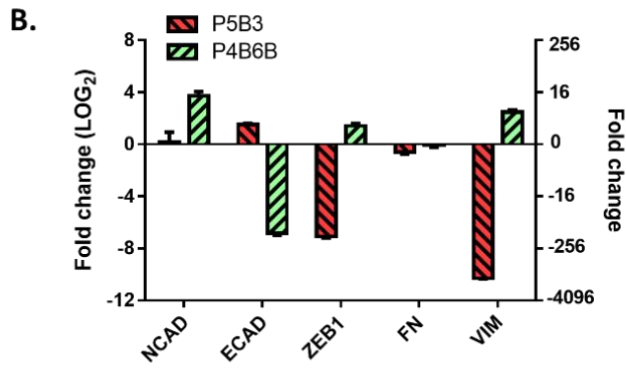
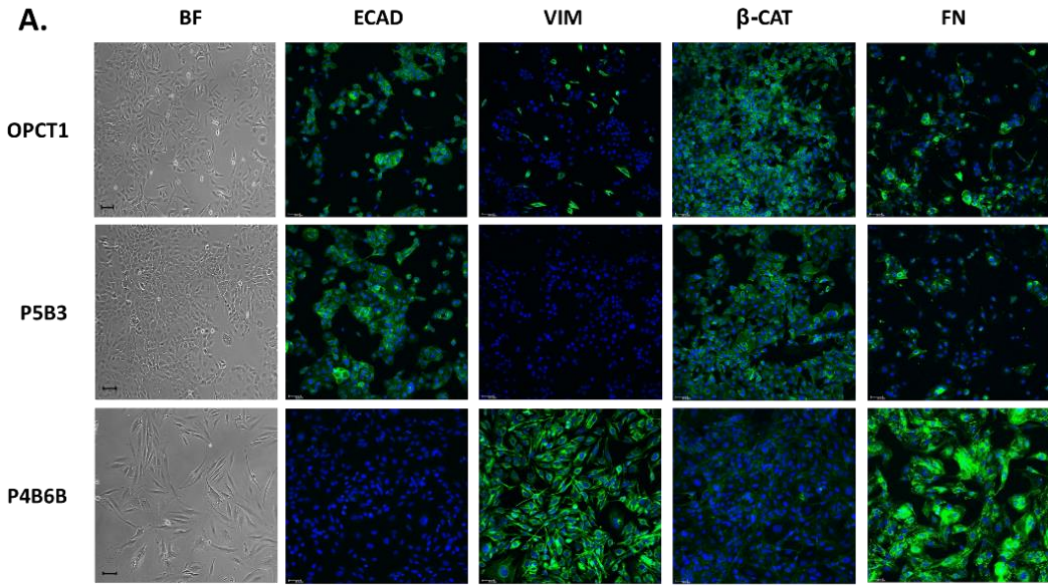


Figure 1. The EMT status of OPCT-1, P5B3 and P4B6B was determined by assessing the expression of epithelial and mesenchymal markers using IF (A), RT-PCR (n=3) (B) and Western blotting (C). in OPCT-1 cells included a CD44^{high}/CD24^{low} sub-population (D) which was not observed in P5B3 (E) or P4B6B (F) cells. The % of CD44^{high}/CD24^{high} and CD44^{high}/CD24^{low} is shown in G and the intensity of expression of each marker/cell line (median fluorescence intensity, MFI) is shown in H (n=3).

The P5B3 clonal progeny form a homogenous cobblestone monolayer, characteristic of an epithelial phenotype. These cells stain positive for the epithelial markers E-cadherin and β -catenin by IF, while exhibiting little/no vimentin expression and variable expression of fibronectin. In contrast, the P4B6B cells are a homogenous population of elongated spindle-like cells, which express reduced levels of E-cadherin/ β -catenin coupled with strong expression of vimentin/fibronectin; hallmarks of a mesenchymal phenotype [7, 9]. In contrast to OPCT-1, P4B6B and P5B3 display homogenous expression for E-cadherin, vimentin and β -catenin, which reflects their clonal origin.

RT-PCR (Fig. 1B) showed P5B3 to express lower levels of the mesenchymal markers, Zeb-1 and vimentin compared to their parental OPCT-1 counterparts. Similarly, P5B3 expresses higher levels of the epithelial marker E-cadherin, with the expression of fibronectin and N-cadherin being similar to that of OPCT-1. P4B6B expression increased levels of mesenchymal markers N-cadherin, Zeb-1 and vimentin, a substantially lower expression of the epithelial marker E-cadherin, but as for P5B3, fibronectin expression (as assessed using RT-PCR) was similar to parental OPCT1. When determined using Western blotting (Fig. 1C), expression of the mesenchymal markers fibronectin and vimentin was higher in P4B6B and lower in P5B3 compared to parental

OPCT1, whereas the opposite was observed for the epithelial markers E-cadherin and β -catenin. Collectively, the phenotypic characterization by IF, RT-PCR and Western blotting confirmed parental OPCT-1 to be a mixed population, whereas P5B3 and P4B6B are epithelial and mesenchymal in nature, respectively. As fibronectin protein expression was shown to follow the trend of P4B6B > OPCT-1 > P5B3, despite little/no difference being detected at the mRNA level, it is likely that post-translational events are responsible for upregulation in P4B6B and OPCT-1, compared to P5B3.

The CD44^{high}/CD24^{low} phenotype is associated with cancer stem cell (CSC)-like cells derived from a variety of cancers, including prostate and breast cancer [26, 27, 28]. The proportion of CD44^{high}/CD24^{low} cells within OPCT-1, P5B3 and P4B6B was determined using flow cytometry. OPCT-1 contained a significant CD44^{high}/CD24^{low} population (~15%) alongside a majority CD44^{high}/CD24^{high} population (~85%) (Fig. 1D). This subpopulation was absent from both P5B3 and P4B6B (Fig. 1E, F), despite their marked differences in epithelial/mesenchymal characteristics (Fig. 1G). This suggests that, in addition to P5B3 (epithelial) and P4B6B (mesenchymal) subpopulations, OPCT-1 contains another (and proportionately large) CD44^{high}/CD24^{low} CSC subpopulation. Median fluorescence intensity (MFI) values (Fig. 1H) show P4B6B expresses a significantly higher intensity of CD44, alongside increased levels of CD24 in comparison to OPCT-1. CD44 (as in the case of integrin receptors) is associated with cell-cell and cell-matrix interactions, and the differential expression within these cell lines may contribute to observed differences in cell adherence capacity [29].

The differential response of cell sub-populations to fluoroalkylsilica.

Live cell imaging was used to compare the responses of defined mesenchymal and epithelial sub-populations and heterogeneous populations towards the fluoroalkylsilica (FS) substrate, a

surface that would be expected to induce disaggregation, particularly for mesenchymal P4B6B cells. On observing cell morphology (Fig. 2A), cultures of P5B3 and OPCT-1 on FS demonstrated delayed adhesion during the early stages of culture (≤ 24 h), after which monolayers formed. This may reflect a transient change in serum proteins at the surface *via* the Vroman effect [30]. The confluency of the P5B3 monolayers progressively increased up to the 96 h time point and their morphology was similar to their counterparts that had been cultured on TCP. In contrast, OPCT-1 contracts into dense ridges by 48 h, and progresses to form a spheroidal morphology by 96 h. These spheroids remain interconnected through long strands of cells. In contrast, P4B6B cells poorly associate with the surface, forming and maintaining a non-adherent spheroidal morphology throughout the 96 h culture period. However, the spheroids are not connected through the tubular projections, as was seen for OPCT-1.

Proliferation assays (Fig. 2B-D) indicate that FS supports the growth of all three cell lines, with growth rates taking the following order: P5B3 > OPCT-1 > P4B6B. In the case of P5B3, proliferation is most likely hindered during the early stages of culture when adherence is disrupted, with some cells possibly undergoing cell death *via* anoikis [31]. Similarly, the proliferation of OPCT-1 on FS is reduced during the first 24 h of culture compared to TCP, the progressive cell-interface dissociation process observed after this (Fig. 2A) does not result in a decrease in the rate of proliferation that is observed after 48 h. The growth of P4B6B is inhibited upon FS throughout the 96 h culture period (compared to that on TCP), reflecting the sustained lack of adherence under these conditions. The slow rate of non-adherent FS growth shown in the case of P4B6B may be permitted through anoikis-resistant properties of these mesenchymal cells [4].

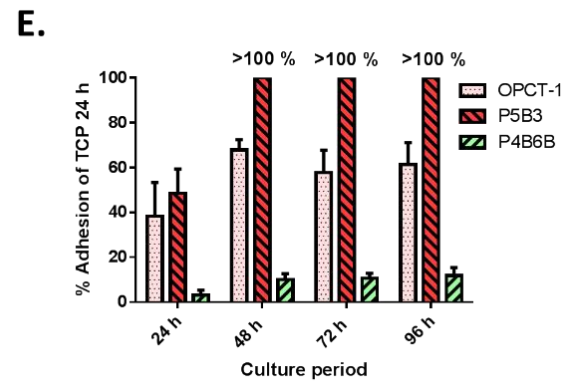
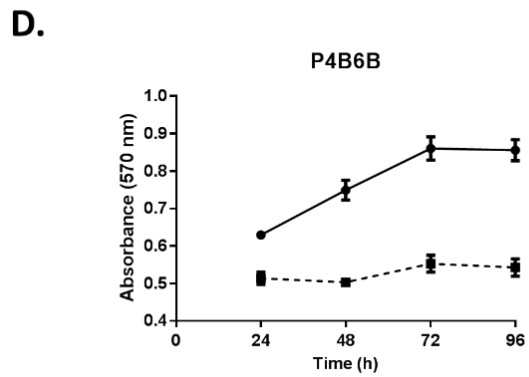
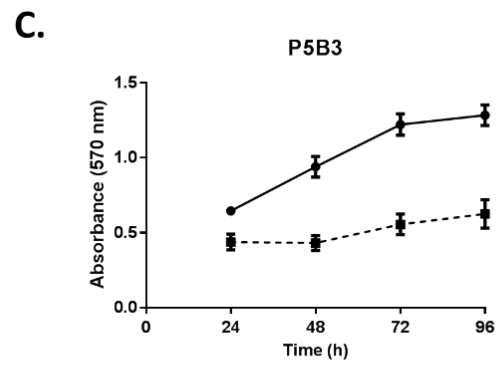
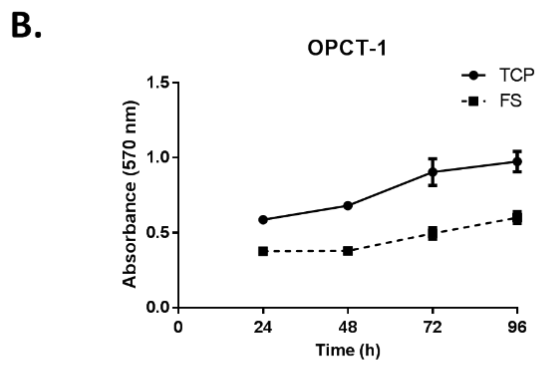
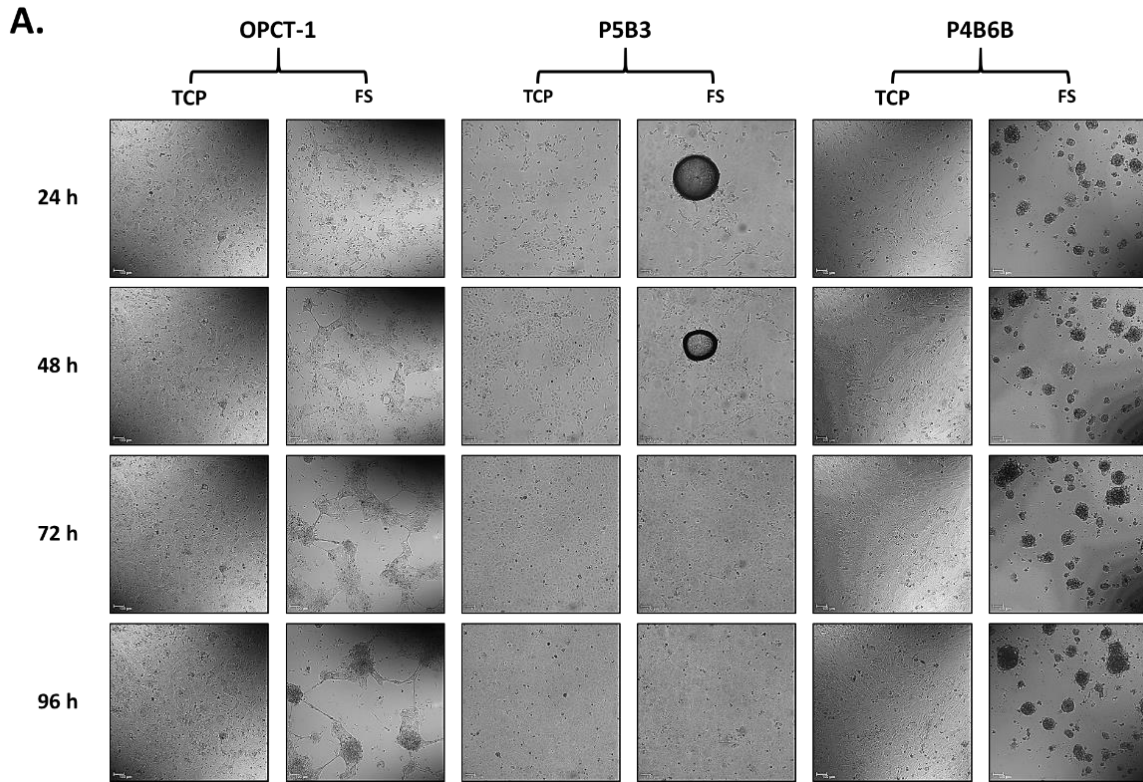


Figure 2. The morphology of OPCT-1, P5B3 and P4B6B cells when cultured upon TCP or FS for 96 h (A). OPCT-1 were shown to associate, and then actively disassociate from FS. P4B6B had little/no association with FS and formed spheroidal aggregates. P5B3 adhered and proliferated upon FS, forming a regular monolayer. The MTT assay (B-D, n=4) revealed a reduction in the proliferation rate of each cell line upon FS, which was most pronounced in the case of P4B6B. Adhesion assays (E, n=8) showed each cell line to be less adherent on FS surfaces in comparison to TCP, with FS adherence following the trend of P5B3 > OPCT-1 >P4B6B.

The MTT assay was used to assess the adherence of each cell line towards FS, with data being normalized to the level of adherence achieved upon TCP after 24 h (Fig. 2E). These data aligned with the proliferation data (Fig. 2B-D), with P5B3 > OPCT-1 > P4B6B. At 24 h, the levels of adherent P5B3 remained below 50% of their TCP counterparts, but increased to exceed this level of adherence after >24 h. OPCT-1 cell adherence was below 40% of TCP counterparts at 24 h, then increased to only ~65% of that achieved upon TCP by 48 h. The level of adherence stabilizes and shows no further increase up to 96 h. P4B6B adherence remains low at only ~10% of TCP counterparts for 24 h, with minimal increase in adherence with time. The morphological, proliferative and adhesion assays show FS supports continual adherent growth of epithelial P5B3, partial/temporary adherent growth for the OPCT-1 parental line, and little/no adherent growth for mesenchymal P4B6B.

The presence of mesenchymal or epithelial populations within OPCT-1, the mesenchymal-like P4B6B and the epithelial-like P5B3 in co-culture was determined based on expression of vimentin, as the characterization data (Fig. 1) demonstrated P5B3 to exhibit little/no vimentin positive cells. This pattern of vimentin expression was confirmed using flow cytometry (Fig. 3). A vimentin^{high}

(mesenchymal) sub-population (~10%) was identified in OPCT-1 which was almost entirely absent from P5B3 (~0.3%), whereas these were the predominant population within P4B6B (>99%).

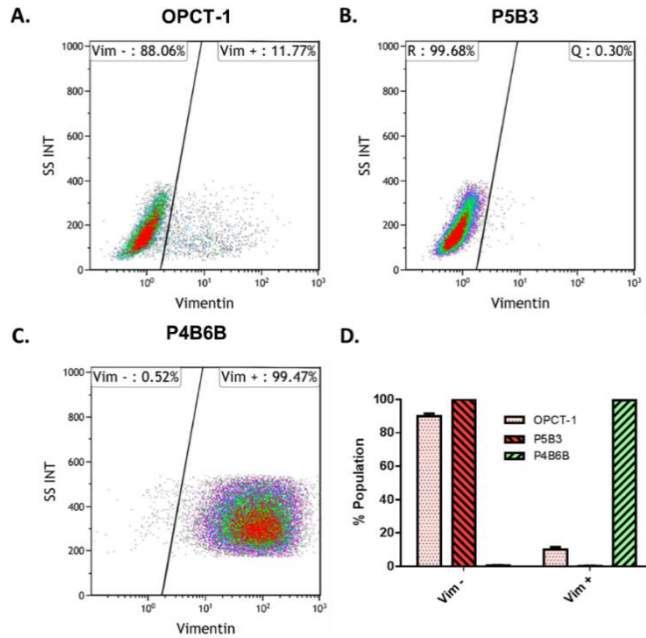


Figure 3. Representative flow cytometry scatter plots displaying the vimentin positive and negative populations within OPCT-1 (A), P5B3 (B) and P4B6B (C). OPCT-1 contains a sub-population of vimentin positive cells (~10%), P5B3 predominantly comprises vimentin negative cells and P4B6B predominantly vimentin positive cells (D, n=3).

If the epithelial/ mesenchymal components of OPCT-1 have no direct influence upon the adherence of one another, then mesenchymal cells could potentially be enriched from FS *via* the non-adherent fraction of the culture. To test this, OPCT-1 was cultured upon FS for 48 h, after which adherent and non-adherent cells were separated and assessed for the expression of the mesenchymal marker vimentin (Fig. 4B-E). Both the non-adherent and adherent fractions of the FS culture (at 48 h) were significantly enriched for a vimentin positive population in comparison

to the parental population (Fig. 4E). In the case of the latter, this unexpected enrichment was attributed to the non-adherent conditions of FS, with more epithelial-like cells undergoing apoptosis through mechanisms such as anoikis, whereas mesenchymal cells are expected to be more inherently resistant to anoikis [4].

Importantly, a proportion (~20-30%) of both the adherent and non-adherent populations following culture on FS were vimentin positive at 48 h, with fractions containing both mesenchymal- and epithelial-like cells (Fig. 4E). This suggests that mesenchymal cells have a heightened ability for FS adhesion when cultured in a mixed population, which contrasts with the observation that pure populations of mesenchymal cells (P4B6B) form non-adherent spheroids when cultured on FS (Fig. 2A, E). Similarly, adherence of epithelial cells to FS may be weakened or disrupted when cultured alongside mesenchymal cells, and this is apparent based on the morphological differences between OPCT-1 and P5B3 shown in Fig. 2A and an explanation for the progressive detachment behavior observed within the mixed OPCT-1 population.

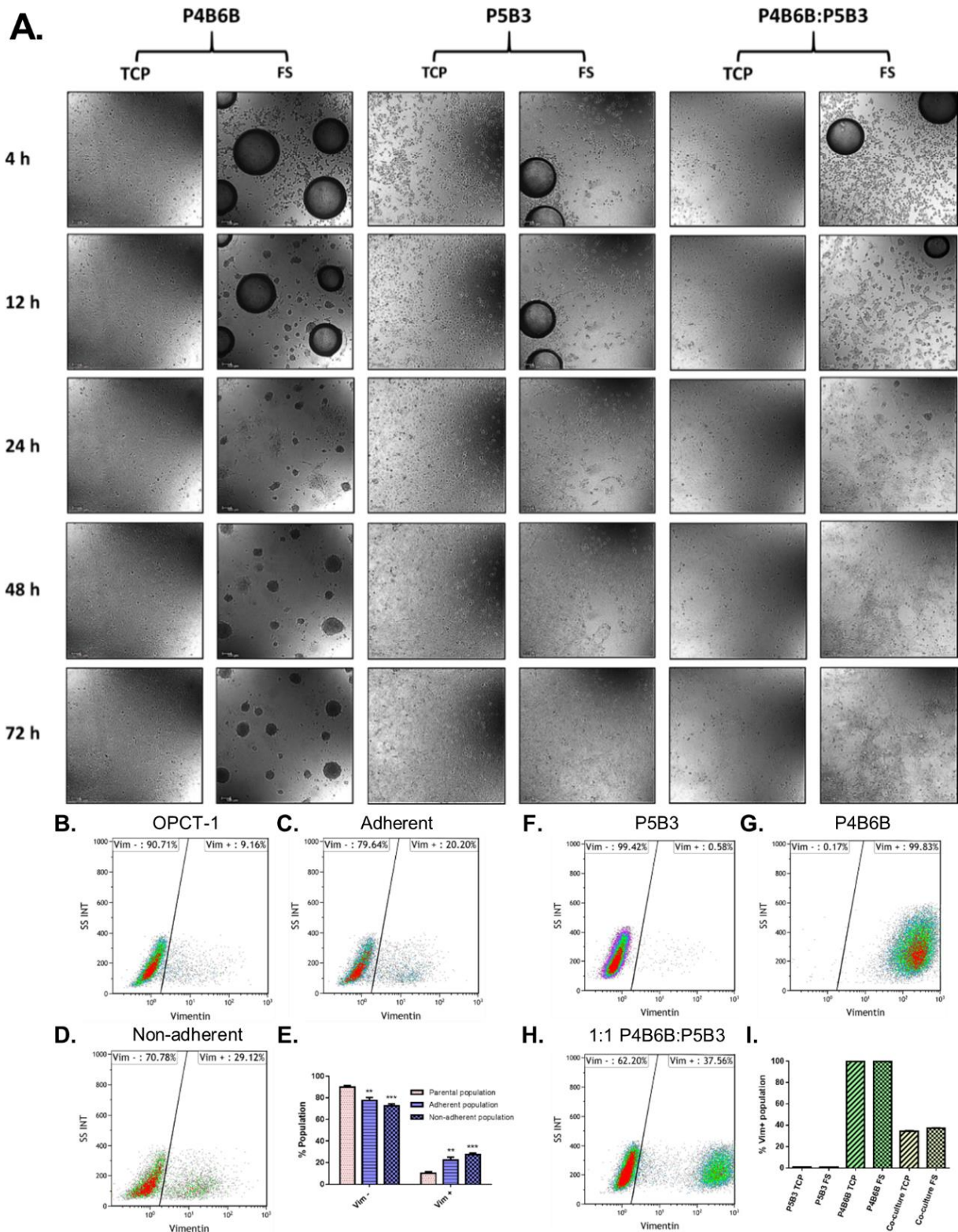


Figure 4. (A) P4B6B form spheroids on FS, in contrast to P5B3. Co-culture of P5B3 and P4B6B (1:1) results in an adherent monolayer, suggesting that the presence of an epithelial sub-population

increases the adherence capability of mesenchymal cells. (B-E) Vimentin expression of OPCT-1 cultured on TCP (B) or FS after 48 h (as assessed by flow cytometry) - the adherent (C) and non-adherent (D) fractions of FS cultures were assessed separately (n=3). Culture on FS enriched for the mesenchymal population, as compared to culture on TCP population (E). The presence of adherent mesenchymal cells in OPCT-1 cultured on FS suggests that the co-culture increases their adhesive capacity. (F-I) Vimentin expression in P5B3 and P4B6B (A, B respectively) is stable after 72 h of culture on FS. The adherent population of P4B6B/P5B3 co-cultured on FS (1:1) contains both vimentin negative and positive cells (C). The percentage of adherent vimentin positive cells in TCP and FS cultures was similar (D, n=3), thereby suggesting that co-culture with P5B3 increases the adhesion of P4B6B when cultured on FS.

P5B3, P4B6B and 1:1 co-cultures were seeded on TCP or FS for 72 h and live cell imaging (Fig. 4A) confirmed that co-culture of P4B6B with P5B3 cells (1:1) increased the adhesion of the former to FS. After removal of the non-adherent population, the presence of a vimentin positive sub-population was assessed using flow cytometry. For P4B6B on FS, only cells from the non-adherent fraction were assessed as there was little/no adherence to FS. These experiments showed little change to the vimentin expression profile of P5B3 or P4B6B when cultured individually upon FS (Fig. 4F, G), suggesting an absence of surface induced changes to vimentin expression on exposure to FS. Accordingly, the adherent fraction of FS co-cultures contained both vimentin positive and negative cells (Fig. 4H), thereby confirming that P4B6B mesenchymal cells adhered to FS in the presence of P5B3 epithelial cells. The adherence of the mesenchymal component on FS as a percentage of the population was similar to that of TCP under standard conditions (~37% vs. ~35%). Although P4B6B mesenchymal cells did not adhere to FS when cultured alone (Fig. 2), adherence was increased when they were co-cultured with P5B3 epithelial cells (Fig. 4).

Discussion

Initial observations suggested a potential application for FS materials as a culture platform for the enrichment of mesenchymal cells by enabling epithelial cells to preferentially adhere. Although an FS-induced enrichment effect was evident (Fig. 4E), we attribute enrichment to the relative sensitivity of cell populations to anoikis-related cues, with mesenchymal cells being less susceptible than epithelial cells. The capacity of low-surface energy FS to enrich mesenchymal cells contrasts well with the capacity of amino-functionalized materials to enrich for epithelial cells [18]. Importantly, the differential responses between sub-populations highlights that the culture environment of pure and mixed mesenchymal/epithelial populations differs significantly irrespective of the culture platform, with each population contributing to the characteristics (e.g. adherence) of the wider/total cell population. Amongst other factors, the influence of mesenchymal cells on the remodeling of ECM is distinct to that of epithelial cells [32]. In the case of FS, a delay in the absorption of adhesion molecules like fibronectin is known, with the initial non-adherent environment becoming adherent due to a suspected Vroman effect [20]. For P4B6B, despite the anticipated Vroman effect and presence of serum, adherence was not recovered, thereby suggesting insensitivity to the adhesion molecules present (Fig. 1A) and that P4B6B adhesion is fibronectin independent (Fig. 2A). The factor which allows P4B6B adherence that is introduced by P5B3 remains unknown, although it is likely to be a cell adhesion or matrix protein which could be identified by analysis of the cell secretome. If identified, then localized induction of this molecule/s may have therapeutic value as it could inhibit intravasation of mesenchymal cells. The organization of the cell types – especially during dynamic events on FS such as that observed for OPCT-1 and P4B6B, could be resolved by an appropriate imaging probe [33].

OPCT-1 consists of multiple epithelial and mesenchymal sub-populations, a distinct CD44^{high}/CD24^{low} sub-population and, likely, others. As P5B3 and P4B6B are clonal progeny of cells that displayed the most pronounced epithelial/mesenchymal phenotypes respectively, they represent populations at the extreme of each phenotypic spectrum [23]. These clonal progenies are therefore a partial representation of OPCT-1, which likely comprises multiple sub-populations at varying stages of EMT and it is plausible for mesenchymal cells to display different adhesive properties to P4B6B. OPCT-1 therefore, in part at least, reflects some of the diversity observed in tumors with respect to EMT states [34] and its progeny represent selected EMT states. Accordingly, the biological response of OPCT-1 and co-cultured P5B3/P4B6B can be expected to differ somewhat. The morphological changes observed for OPCT-1, when cultured upon FS, were not apparent in P5B6:P4B6B co-cultures at 72 h (Fig. 2A, 4A), despite a higher proportion of mesenchymal cells (50% vs. ~ 10%) in the co-cultures. Mesenchymal cells may not drive epithelial dissociation, perhaps due to the inherent complexity of OPCT-1 in comparison to P5B3 and P4B6B, as discussed above. The CD44^{high}/CD24^{low} component of OPCT-1 (which may also influence bulk cellular adherence) was not present in the co-cultures. Furthermore, P5B3 may be more resistant to the influence of a mesenchymal sub-population than the bulk of the epithelial population within OPCT-1, due to the nature in which the clonal ancestor of P5B3 was selected [23]. The progressive dissociation observed in OPCT-1 cultures on FS is interesting as it provides supportive evidence for a tumor cell cooperativity and collective cell migration theory as an explanation for the origin and mixed phenotype observed in circulating tumor cell clusters, as under certain conditions normally adherent bulk of cells can be induced to lose contact [35].

Marked differences in the adherence of epithelial and mesenchymal sub-populations to FS surfaces were observed, suggesting that cell differentiation status directly influences adherence

capability. Although EMT is linked to drug- and apoptosis-resistance and an increased capacity for motility [7, 19], the response to FS observed in co-culture demonstrates that mesenchymal/epithelial cells can influence the adherence of other sub-populations. In relation to metastasis, our observations provide an insight into how EMT sub-populations could influence cell attachment/detachment *in vivo*. It can be inferred that specific sub-populations alter adhesive events in the local microenvironment over time, possibly *via* mechanisms such as ECM breakdown (matrix metalloproteinase secretion) or remodeling (secretion of ECM components) [36]. Importantly, none of these differential adherence characteristics were observed for cells cultured on conventional TCP. Although FS (as TCP) poorly reflects *in vivo* tissues, similar processes relating to the establishment and modelling of the local microenvironment are likely to occur *in vivo*. We proposed that attempts to observe such phenomena within animal models might be challenging, highlighting the utility of alternate culture platforms for *in vitro* research.

Conclusion

OPCT-1 is a heterogeneous prostate cancer cell line derived from primary (rather than metastatic) disease which contains epithelial, mesenchymal and CD44^{high}/CD24^{low} cancer stem cell sub-populations. We demonstrate that OPCT-1 cells adherent to FS surfaces comprise both epithelial- and mesenchymal-like populations. In contrast, a mesenchymal sub-population derived from OPCT1 (P4B6B) poorly adhered to FS and formed spheroids, whereas an epithelial sub-population derived from OPCT1 (P5B3) formed an adherent monolayer. However, P4B6B did adhere to FS when co-cultured with P5B3. Taken together, these findings demonstrate that EMT/cell differentiation status dictates cell adhesive capacity and provide a novel insight into the relationship between epithelial and mesenchymal cell populations in stages of metastasis such as

intravasation. Importantly, the differences in adherence capacity between P4B6B and P5B3 were not apparent using standard TCP-based culture, thereby highlighting the value of using alternative culture surfaces for studying cell surface interaction/adhesion phenomena and interrogating mechanisms involved in adhesion and detachment of metastatic tumor cells.

ASSOCIATED CONTENT

Supporting Information.

Supplementary information (PDF) containing RT-PCR primer information, immunofluorescence, flow cytometry gating and live cell imaging video.

Corresponding Author

*Corresponding author. Email: carole.perry@ntu.ac.uk Tel: 0115 848 6695

Author Contributions

The manuscript was written through contributions of all authors. All authors have given approval to the final version of the manuscript.

Funding Sources

An NTU QR-funded Vice Chancellors Competitive PhD Scholarship to M. Nicklin and the John and Lucille van Geest Foundation supported this work.

ACKNOWLEDGMENT

The authors acknowledge Dr S.E.B McArdle and Dr G.A. Foulds for assistance with flow cytometry and Prof. R.C. Rees, Mr S. Reeder and Mrs A. Schneider for their invaluable intellectual and technical support and contributions.

ABBREVIATIONS

CCR2, CC chemokine receptor 2; CCL2, CC chemokine ligand 2; CCR5, CC chemokine receptor 5; TLC, thin layer chromatography.

REFERENCES

1. Hong, M.K.H.; Macintyre, G.; Wedge, D.C.; Van Loo, P.; Patel, K.; Lunke, S.; Alexandrov, L.B.; Sloggett, C.; Cmero, M.; Marass, F.; Tsui, D.; Mangiola, S.; Lonie, A.; Naeem, H.; Sapre, N.; Phal, P.M.; Kurganovs, N.; Chin, X.; Kerger, M.; Warren, A.Y.; Neal, D.; Gnanapragasam, V.; Rosenfeld, N.; Pedersen, J.S.; Ryan, A.; Haviv, I.; Costello, A.J.; Corcoran, N.M.; Hovens, C.M. Tracking the origins and drivers of subclonal metastatic expansion in prostate cancer. *Nat. Commun.* 2015, 6, 6605.
2. Kalluri, R.; Neilson, E.G. Epithelial-mesenchymal transition and its implications for fibrosis. *J. Clin. Invest.* 2003, 112, 1776–1784.
3. Duband, J.L. Diversity in the molecular and cellular strategies of epithelium-to-mesenchyme transitions: Insights from the neural crest. *Cell Adh. Migr.* 2010, 4, 458-482.
4. Paoli, P.; Giannoni, E.; Chiarugi, P. Anoikis molecular pathways and its role in cancer progression. *Biochim. Biophys. Acta – Mol. Cell Res.* 2013, 1833, 3481-3498.

5. Figiel, S.; Vasseur, C.; Bruyere, F.; Rozet, F.; Maheo, K.; Fromont, G. Clinical significance of epithelial-mesenchymal transition markers in prostate cancer. *Hum. Pathol.* 2017, 61, 26-32.
6. Satelli, A.; Bath, I.; Brownlee, Z.; Mitra, A.; Zhou, S.; Noh, H.; Rojas, C.R.; Li, H.; Meng, Q.H.; Li, S. EMT circulating tumor cells detected by cell-surface vimentin are associated with prostate cancer progression. *Oncotarget.* 2017, 8, 49329-49337.
7. Voulgari, A.; Pintzas, A. Epithelial–mesenchymal transition in cancer metastasis: Mechanisms, markers and strategies to overcome drug resistance in the clinic. *Biochim. Biophys. Acta* 2009, 1796, 75-90.
8. Farfán, N.; Ocarez, N.; Castellón, E.A.; Mejía, N.; García de Herreros, A.; Contreras, H.R. The transcriptional factor ZEB1 represses Syndecan 1 expression in prostate cancer. *Sci. Rep.* 2018, 8, 11467.
9. Jiang, Y.; Luo, Y.; He, D.; Li, X.; Zhang, L.; Peng, T.; Li, M.; Lin, Y. Role of Wnt/ β -catenin signaling pathway in epithelial-mesenchymal transition of human prostate cancer induced by hypoxia-inducible factor-1 α . *Int. J. Urol.* 2007, 14, 1034-1039.
10. Šimečková, Š.; Kahounová, Z.; Fedr, R.; Remšík, J.; Slabáková, E.; Suchánková, T.; Procházková, J.; Bouchal, J.; Kharaishvili, G.; Král, M.; Beneš, P.; Souček, K. High Skp2 expression is associated with a mesenchymal phenotype and increased tumorigenic potential of prostate cancer cells. *Sci. Rep.* 2019, 9, 5695.
11. Lamouille, S.; Xu, J.; Derynck, R. Molecular mechanisms of epithelial-mesenchymal transition. *Nat. Rev. Mol. Cell Bio.* 2014, 15, 178-196.

12. Sutherland, M.; Gordon, A.; Shnyder, S.D.; Patterson, L.H.; Sheldrake, H.M. RGD-Binding integrins in prostate cancer: expression patterns and therapeutic prospects against bone metastasis. *Cancers* 2012, 4, 1106-1145.
13. Zoni, E.; van der Horst, G.; van de Merbel, A.F.; Chen, L.; Rane, J.K.; Pelger, R.C.M.; Collins, A.T.; Visakorpi, T.; Snaar-Jagalska, B.E.; Maitland, N.J.; van der Pluijm, G. miR-25 modulates invasiveness and dissemination of human prostate cancer cells via regulation of α v- and α 6-integrin expression. *Cancer Res.* 2015, 75, 2326-2336.
14. Balcioglu, H.E.; van Hoorn, H.; Donato, D.M.; Schmidt, T.; Danen, E.H.J. The integrin expression profile modulates orientation and dynamics of force transmission at cell–matrix adhesions. *J. Cell Sci.* 2015, 128, 1316-1326.
15. Pan, B.; Guo, J.; Liao, Q.; Zhao, Y. β 1 and β 3 integrins in breast, prostate and pancreatic cancer: A novel implication. *Oncol. Lett.* 2018, 15, 5412-5416.
16. Griffin, M.F.; Ibrahim, A.; Seifalian, A.M.; Butler, P.E.M.; Kalaskar, D.M.; Ferretti, P. Chemical group-dependent plasma polymerisation preferentially directs adipose stem cell differentiation towards osteogenic or chondrogenic lineages. *Acta Biomater.* 2017, 50, 450-461.
17. Roach, P.; Farrar, D.; Perry, C.C. Surface tailoring for controlled protein adsorption: effect of topography at the nanometer scale and chemistry. *J. Am. Chem. Soc.* 2006, 128, 3939-3945.

18. Hickman, G.J.; Rees, R.C.; Boocock, D.J.; Pockley, A.G.; Perry, C.C. Controlling the dynamics of cell transition in heterogeneous cultures using surface chemistry. *Adv. Healthc. Mater.* 2015, 4, 593-601.
19. Katsuno, Y.; Meyer, D.S.; Zhang, Z.; Shokat, K.M.; Akhurst, R.J.; Miyazono, K.; Derynck, R. Chronic TGF- β exposure drives stabilized EMT, tumor stemness, and cancer drug resistance with vulnerability to bitopic mTOR inhibition. *Sci. Signal.* 2019, 12, eaau8544.
20. Nicklin, M.; Rees, R.C.; Pockley, A.G.; Perry, C.C. Development of an hydrophobic fluoro-silica surface for studying homotypic cancer cell aggregation-disaggregation as a single dynamic process in vitro. *Biomater. Sci.* 2014, 2, 1486–1496.
21. Schröder, F.H.; Hugosson, J.; Roobol, M.J.; Tammela, T.L.J.; Zappa, M.; Nelen, V.; Kwiatkowski, M.; Lujan, M.; Määttänen, L.; Lilja, H.; Denis, L.J.; Recker, F.; Paez, A.; Bangma, C.H.; Carlsson, S.; Puliti, D.; Villers, A.; Rebillard, X.; Hakama, M.; Stenman, U-H.; Kujala, P.; Taari, K.; Aus, G.; Huber, A.; van der Kwast, T.H.; van Schaik, R.H.N.; Koning, H.J.; Moss, S.M.; Auvinen, A. Screening and prostate cancer mortality: results of the European Randomised Study of Screening for Prostate Cancer (ERSPC) at 13 years of follow-up. *Lancet.* 2014, 384, 2027-2035.
22. Ost, P.; Reynders, D.; Decaestecker, K.; Fonteyne, V.; Lumen, N.; de Bruycker, A.; Lambert, B.; Delrue, L.; Bultijnck, R.; Claeys, T.; Goetghebeur, E.; Villeirs, G.; de Man, K.; Ameye, F.; Billiet, I.; Joniau, S.; Vanhaverbeke, F.; de Meerleer, G. Surveillance or metastasis-directed therapy for oligometastatic prostate cancer recurrence: A prospective, randomized, multicenter Phase II Trial. *J. Clin. Oncol.* 2018, 36, 446-453.

23. Harner-Foreman, N.; Vadakekolathu, J.; Laversin, S.A.; Mathieu, M.G.; Reeder, S.; Pockley, A.G.; Rees, R.C.; Boocock, D.J. A novel spontaneous model of epithelial-mesenchymal transition (EMT) using a primary prostate cancer derived cell line demonstrating distinct stem-like characteristics. *Sci. Rep.* 2017, 7, 40633.
24. Palazzolo, A.; Heng, H.; Mohammad, R.; Theocharous, P.; Eliason, J.F. Characterization of three pairs of prostate cells lines derived from tumour and adjacent normal tissues. *Proc. Amer. Assoc. Cancer Res.* 2005, 65, 462.
25. Pfaffl, M.W. A new mathematical model for relative quantification in real-time RT-PCR. *Nucleic Acids Res.* 2001, 29, e45.
26. Davies, A.H.; Beltran, H.; Zoubeidi, A. Cellular plasticity and the neuroendocrine phenotype in prostate cancer. *Nat. Rev. Urol.* 2018, 15, 271-286.
27. Fillmore, A.; Kuperwasser, C. Human breast cancer stem cell markers CD44 and CD24: enriching for cells with functional properties in mice or in man? *Breast Cancer Res.* 2007, 9, 303.
28. Hurt, E.M.; Kawasaki, B.T.; Klarmann, G.J.; Thomas, S.B.; Farrar, W.L. CD44⁺CD24⁻ prostate cells are early cancer progenitor/stem cells that provide a model for patients with poor prognosis. *Br. J Cancer.* 2008, 98, 756-765.
29. Senbanjo, L.T.; Chellaiah, M.A. CD44: A multifunctional cell surface adhesion receptor is a regulator of progression and metastasis of cancer cells. *Front. Cell Dev. Biol.* 2017, 7, 18.

30. Vroman, L.; Adams, A.L. Adsorption of proteins out of plasma and solutions in narrow spaces. *J. Colloid Interface Sci.* 1986, 111, 391-402.
31. Tzanakakis, G.; Kavasi, R.; Voudouri, K.; Berdiaki, A.; Spyridaki, I.; Tsatsakis, A.; Nikitovic, D. Role of the extracellular matrix in cancer-associated Epithelial to Mesenchymal Transition phenomenon. *Dev. Dyn.* 2018, 247, 368-381.
32. Zhang, P.; Chen, L.; Song, Y.; Li, X.; Sun, Y.; Xiao, Y.; Xing, Y. Tetraiodothyroacetic acid and transthyretin silencing inhibit pro-metastatic effect of L-thyroxin in anoikis-resistant prostate cancer cells through regulation of MAPK/ERK pathway. *Exp. Cell Res.* 2016, 347, 350-359.
33. Lee, Y.; Kim, J.; Lee, J.; Lee, J.H.J.; Sahu, S.; Kwon, H.; Park, S.; Jang, S.; Lee, J.; Wang, Z.; Tam, W.L.; Lim, B.; Kang, N.; Chang, Y. Identification of tumor initiating cells with a small-molecule fluorescent probe by using vimentin as a biomarker. *Angew. Chem.* 2018, 57, 2851-5854.
34. Pastushenko, I.; Brisebarre, A.; Sifrim, A.; Fioramonti, M.; Revenco, T.; Boumahdi, S.; Van Keymeulen, A.; Brown, D.; Moers, V.; Lemaire, S.; De Clercq, S.; Minguijón, E.; Balsat, C.; Sokolow, Y.; Dubois, C.; De Cock, F.; Scozzaro, S.; Sopena, F.; Lanas, A.; D'Haene, N.; Salmon, I.; Marine, J-C.; Voet, T.; Sotiropoulou, P.A.; Blanpain, C. Identification of the tumour transition states occurring during EMT. *Nature.* 2018, 556, 463-468.
35. Giuliano, M.; Shaikh, A.; Lo, H.C.; Arpino, G.; De Placido, S.; Zhang, X.H.; Cristofanilli, M.; Schiff, R.; Trivedi, M.V. Perspective on circulating tumor cell clusters: Why it takes a village to metastasize. *Cancer Res.* 2018, 78, 845-852.

36. Smith, B.N.; Bhowmick, N.A. Role of EMT in metastasis and therapy resistance. *J. Clin. Med.* 2016, 5, 1-17.